Dyakonov surface waves at interface between hexagonal-boron-nitride and isotropic material

B Zhu[1,2,3], G Ren[1,2,*], Y Gao[1,2], Q Wang,[3], C Wan,[3] J Wang,[4] and S Jian[1,2]

[1]Key Lab of All Optical Network & Advanced Telecommunication Network of EMC, Beijing Jiaotong University, Beijing 100044, China

[2]Institute of Lightwave Technology, Beijing Jiaotong University, Beijing 100044, China

[3]Department of Electrical and Electronic Engineering, University of Bristol, Bristol, UK

[4]Science and Technology on Optical Radiation Laboratory, Beijing 100854, China

E-mail: gbren@bjtu.edu.cn

Abstract In this paper we analyze the propagation of Dyakonov surface waves (DSWs) at the interface between hexagonal-boron-nitride (h-BN) and isotropic dielectric material. Various properties of DSWs supported at the dielectric-elliptic and dielectric-hyperbolic types of interfaces have been theoretically investigated, including the real effective index, the propagation length, the angular existence domain (AED) and the composition ratio of evanescent field components in h-BN crystal and isotropic dielectric material, respectively. The analysis in this paper reveals that the h-BN could be a promising anisotropic material to observe the propagation of DSWs and may have potentials in diverse applications, such as the high sensitivity stress sensing or the optical sensing of analytes infiltrating dielectric materials.

Keywords**:** Dyakonov surface waves, h-BN, anisotropic mediums.

PACS: 73.20.Mf

Introduction

Electromagnetic surface waves are special types of excitations, which enables the confinement of light at the boundary between two different mediums with its amplitude exponentially decaying along out-of-plane direction [1]. Depending on the types of mediums forming interface, various categories of electromagnetic surface waves are supported, such as the surface plasmon polaritons

on graphene (GPs) [2-6], the surface phonon polaritons (SPhPs) [7-8], the nonlinear surface waves [9-12] and the Dyakonov surface waves (DSWs) [13-14]. Within these surface waves, the DSWs are distinctive since their presence is due to the difference between the symmetry of two mediums [13-14], wherein at least one has to be anisotropic. The most fascinating property of DSWs is that such surface waves could propagate between transparent mediums, therefore they are lossless when the dielectric loss is neglected [15].

Although DSWs were theoretically predicted nearly three decades ago, while it took 20 years until they were finally experimentally observed [16] due to the stringent requirement of high degree of birefringence in anisotropic medium, which does not commonly occur in naturally available materials. So far, the DSWs have been theoretically investigated in a great variety of schemes, wherein either the anisotropic medium or the isotropic medium was replaced. For the cases where only the transparent anisotropic medium was replaced, various anisotropic mediums including the biaxial crystal [17], the structurally chiral material [18], the hyperbolic metamaterial [19] or an anisotropic and nonhomogeneous media [20] have been reported. The DSWs at the interfaces between dielectric birefringent media and alternative isotropic mediums were also studied, in which the isotropic medium could be the magnetic media [22] or the left-handed materials [23]. However, for the biaxial crystal or chiral material, tiny birefringence restricts the propagation of DSWs and ensures they can only be supported in a narrow angular existence domain (AED). Although hyperbolic metamaterials with large birefringence were proposed to relax the directivity of DSWs [19], the intrinsic plasmonic loss impair the performance of DSWs and the fabrication of metamaterials requires complicated procedure [21].

Previously, the DSWs at the interfaces of dielectric-elliptic and dielectric-hyperbolic types have been theoretically analysed [24] with the intrinsic loss of artificial hyperbolic metamaterials was ignored. However, in practical applications, considerable plasmonic loss exists in the metal-dielectric metamaterials [25]. Ignoring the intrinsic loss of artificial metamaterials simply makes [24] more like a purely theoretical study. Instead, investigating the propagation of DSWs between lossy anisotropic and isotropic mediums would make it more compatible with the experimental study of DSWs and valuable to the field. Secondly, the fabrication procedure of artificial hyperbolic metamaterials is quite complex and challenging. The hyperbolic material with acceptable intrinsic loss and simple fabrication procedure is highly recommended.

Recently, it has been found that hexagonal boron nitride (h-BN), a natural hyperbolic material, exhibits an extreme anisotropy due to its weak van der Waals bonded nature [26]. Compared with the artificial hyperbolic metamaterials, h-BN possesses much lower loss [27], which makes the h-BN a more competitive platform to study the propagation of DSWs. Meanwhile, recent study has found the extreme anisotropy of h-BN is still sustained even for the h-BN slab with thickness down to several nanometers [26], which might allow one to cross over the regimes beyond the simple effective medium theory in artificially engineered metamaterials. Furthermore, since both the elliptical and hyperbolical dispersion relationships can be found in h-BN [28], the DSWs can be supported at dielectric-elliptic or dielectric-hyperbolic interface types, which greatly improves its flexibility in studying the propagation of DSWs modes. Finally, the h-BN can be grown in large area using CVD techniques [29]. All of these properties make h-BN a promising anisotropic material to study the DSWs.

In this paper, we investigate the propagation of Dyakonov surface waves (DSWs) at the interface between hexagonal-boron-nitride and isotropic dielectric material. In the second section, the propagation of DSWs at two types of interfaces, *i.e.* the dielectric-elliptic and dielectric-hyperbolic interfaces, are discussed. The theoretical expressions of propagation constant, the direction angle of wave vector, the angular existence domain (AED), the composition ratio between transverse-magnetic (TM) and transverse-electric (TE) waves in dielectric material and between extraordinary and ordinary modes in h-BN are respectively derived. In the third and fourth section, theoretical results corresponding to the DSWs at dielectric-elliptic and dielectric-hyperbolic interfaces under different wavenumbers or isotropic dielectric material permittivities

are presented. In the end we draw conclusions.

2.Models and Materials

The sketch shown in Fig. 1 is the Dyakonov surface waves supported at the interface between h-BN and isotropic dielectric material. The optics axis (OA) of h-BN crystal is parallel to the interface. The h-BN crystal is located in the half-space $x<0$ while the anisotropic dielectric material with complex permittivity ε_d is located in the half space $x>0$. The permittivities parallel and normal to the optics axis of h-BN is respectively set as $\varepsilon_{\parallel}$ and $\varepsilon_{\perp}$, which can be described by a single Lorentzian [26],

$$\varepsilon_{\mu} = \varepsilon_{\infty,\mu} + \varepsilon_{\infty,\mu} \frac{(\omega_{LO,\mu})^2 - (\omega_{TO,\mu})^2}{(\omega_{TO,\mu})^2 - \omega^2 - i\omega\Gamma_{\mu}}, \mu = \parallel (\perp) \tag{1}$$

where two kinds of phonon modes are related to the intrinsic hyperbolicity in h-BN, namely out of plane phonon modes with $\omega_{TO,\parallel}$=780 cm^{-1}, $\omega_{LO,\parallel}$=830 cm^{-1} and in-plane phonon modes with $\omega_{TO,\perp}$=1370 cm^{-1}, $\omega_{LO,\perp}$=1610 cm^{-1} [28]. Other parameters are chosen as $\varepsilon_{\infty,\parallel}$=2.95, $\varepsilon_{\infty,\perp}$=4.87, $\Gamma_{\parallel}$=4 cm^{-1} and $\Gamma_{\perp}$=5 cm^{-1}, which are from previous measurements [30]. For a better presentation, the aforementioned permittivity tensor components of h-BN as functions of wavenumbers are plotted in Fig. 1(b). It is well-known that h-BN support two distinct Reststrahlen (RS) bands, wherein lower (780 cm^{-1}<ω<830 cm^{-1}) and upper (1370 cm^{-1} <ω<1610 cm^{-1}) RS bands exhibit type-I ($\varepsilon_{\perp}>0$, $\varepsilon_{\parallel}<0$) and type-II ($\varepsilon_{\perp}<0$, $\varepsilon_{\parallel}>0$) hyperbolicity. In contrast, the dispersion relationships in h-BN outside the RS bands are elliptical. Specifically, as shown in Fig. 1(b), two categories of relationships between $\varepsilon_{\parallel}$ and $\varepsilon_{\perp}$ can be found in elliptical dispersion region, namely $\varepsilon_{\parallel} > \varepsilon_{\perp} > 0$ (746 cm^{-1}<ω<780 cm^{-1}, 1610 cm^{-1}<ω<1700 cm^{-1}) and $\varepsilon_{\perp} > \varepsilon_{\parallel} > 0$ (600 cm^{-1}<ω<746 cm^{-1}, 830 cm^{-1}<ω<1370 cm^{-1}). Based on the previous study [13,24], for the anisotropic material with elliptical dispersions, the DSWs only exist at the dielectric-elliptic interface under $\varepsilon_{\parallel} > \varepsilon_d > \varepsilon_{\perp}$ and once the isotropic material is with hyperbolic dispersions, the dielectric-hyperbolic interface supports the propagation of DSWs under $-\varepsilon_{\perp}{}^* > \varepsilon_d > 0$, regardless of $-\varepsilon_{\perp}{}^* > \varepsilon_{\parallel}$ or $-\varepsilon_{\perp}{}^* < \varepsilon_{\parallel}$. Therefore, in this paper, we only focus on the two most representative frequency regions, 750 cm^{-1}<ω<775 cm^{-1} for DSWs on dielectric-elliptic interface and 1380 cm^{-1}<ω<1580 cm^{-1} for DSWs on dielectric-hyperbolic interface.

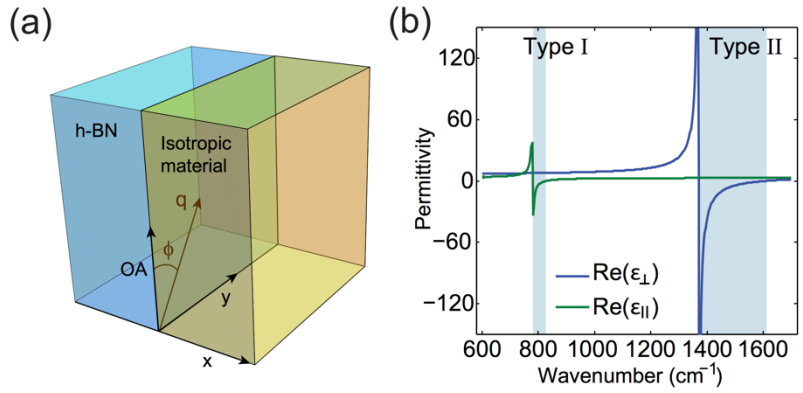

Figure 1. (a) Schematic view of the propagation of DSWs at the interface between the h-BN and an isotropic dielectric material. The propagation direction of wave vector is marked via black arrow. The intersection angles between vectors and optics axis (OA) of h-BN are denoted as ϕ. (b) Permittivity tensor components of h-BN, in which two types of Reststrahlen (RS) bands are marked.

It is well known that the DSWs are hybrid modes with the polarization hybridization involves

four evanescent fields, two field modes corresponding to both transverse-magnetic (TM) and transverse-electric (TE) waves in isotropic dielectric and the other two field modes corresponding to the ordinary and extraordinary modes in h-BN crystal. Assuming the in-plane components of these four evanescent fields are continuous along the interface between two different medias (*i.e.* plane x=0), we obtain the relationship below [13],

$$(k_e - k_o)\left[(k_d + k_e)(k_d + k_o)(\varepsilon_d k_o + \varepsilon_\perp k_e) - (\varepsilon_\parallel - \varepsilon_d)(\varepsilon_d - \varepsilon_\perp)k_o\right] = 0, \tag{2}$$

where the wave vectors k_d, k_o (k_e) represent the out-plane wave vectors of the evanescent fields in isotropic dielectric material and the ordinary (extraordinary) modes in h-BN crystal. Note that in our discussions, all wave vectors are normalized by the free-space wavenumber k_0 and can be calculated through the equation below [13],

$$\begin{aligned} &k_d^2 = q^2 - \varepsilon_d, k_o^2 = q^2 - \varepsilon_\perp, \\ &(q^2 \sin^2\phi - k_e^2)/\varepsilon_\parallel + q^2\cos^2\phi/\varepsilon_\perp = 1, \end{aligned} \tag{3}$$

where the parameter q indicates the propagation constant of DSWs, the parameter ϕ denotes the direction angle of DSWs. Assuming the precondition of $k_e \neq k_o$ is satisfied in Eq. (2), we have the transcendental Dyakonov equation, which is shown below and denoted as Eq. (4). By substituting Eq. (3) into it, the propagation constant of DSWs q can be derived.

$$(k_d + k_e)(k_d + k_o)(\varepsilon_d k_o + \varepsilon_\perp k_e) = (\varepsilon_\parallel - \varepsilon_d)(\varepsilon_d - \varepsilon_\perp)k_o. \tag{4}$$

For the convenience of distinguishing the polarization characteristics of DSWs, we define two quantities, $P_{O/E}$ and $P_{E/M}$. The quantity $P_{O/E}$ represents the absolute amplitude ratios of ordinary modes to extraordinary modes in h-BN. And the quantity $P_{E/M}$ denotes the absolute amplitude ratios of the TE modes to the TM modes in isotropic dielectric material. These two quantities can be also derived through the continuity of electromagnetic field components at the interface, which are shown below,

$$P_{O/E} = \left|\frac{i\tan\phi(k_d + k_e)}{\varepsilon_\perp - q^2 - k_o k_d}\right|, \tag{5}$$

$$P_{E/M} = \left|\frac{q^2 - k_o k_e - \varepsilon_\perp}{i\varepsilon_\perp(k_e + k_d)\tan\phi + ik_e(\varepsilon_\perp - q^2 - k_o k_d)\cot\phi}\right|. \tag{6}$$

Now we first focus on the case of propagation of DSWs at the interface of dielectric-elliptic type. The limits of direction angle ϕ of the propagating DSWs, ϕ_1 and ϕ_2, can be derived by respectively letting k_d=0 and k_e=0 [13],

$$\sin^2\phi_1 = \frac{\varepsilon_d - \varepsilon_\perp}{2(\varepsilon_\parallel - \varepsilon_\perp)}\left[1 - \frac{\varepsilon_d - \varepsilon_\perp}{\varepsilon_\perp} + \sqrt{\left(1 - \frac{\varepsilon_d - \varepsilon_\perp}{\varepsilon_\perp}\right)^2 + \frac{4(\varepsilon_\parallel - \varepsilon_\perp)}{\varepsilon_\perp}}\right], \tag{7}$$

$$\sin^2\phi_2 = \frac{\varepsilon_\parallel^3(\varepsilon_d - \varepsilon_\perp)}{(\varepsilon_\parallel - \varepsilon_\perp)\left[\varepsilon_d\varepsilon_\parallel^2 - \varepsilon_\perp(\varepsilon_\parallel - \varepsilon_d)^2\right]}. \tag{8}$$

It also worth noting that the tenability of the dispersion equation Eq. (4) depends on the precondition of $k_e \neq k_o$. Once it fails, there may be a singularity point in the dispersion space, corresponding to the direction angle of ϕ_{sp}, which can be obtained by letting $k_e = k_o$ [24],

$$\cos^2\phi_{sp} = \varepsilon_\perp / m_3, \tag{9}$$

where m_3 can be expressed as,

$$m_3 = \frac{\varepsilon_d - \varepsilon_\perp}{4}\left[\frac{\varepsilon_\parallel - \varepsilon_d}{\varepsilon_d + \varepsilon_\perp} + \frac{\varepsilon_d + \varepsilon_\perp}{\varepsilon_\parallel - \varepsilon_d}\right] + \frac{\varepsilon_d + \varepsilon_\perp}{2}. \tag{10}$$

Next we turn into the case of propagation of DSWs at the interface of dielectric-hyperbolic type. Compared to the case of dielectric-elliptic interface, the propagation of DSWs still obeys Eqs. (1-6). However, as the requirement of relationship between $\varepsilon_\parallel$, ε_d and $\varepsilon_\perp$ for the propagation of DSWs is relaxed, the direction angle limits of wave vectors need to be redefined. The lower limit of direction angle ϕ is obtained by choosing an infinite large q as the propagation constant [31],

$$\sin^2\phi_3 = \frac{\varepsilon_d^2 - \varepsilon_\perp^*\varepsilon_\parallel}{-\varepsilon_\perp^*(\varepsilon_\parallel - \varepsilon_\perp^*)}, \tag{11}$$

where $\varepsilon_\perp{}^*$ is the conjugate of permittivity $\varepsilon_\perp$.The upper limit of direction angle depends on the relative magnitude between the permittivity ε_d and the benchmark permittivity $\chi=-\varepsilon_\parallel\varepsilon_\perp{}^*/(\varepsilon_\parallel-\varepsilon_\perp{}^*)$, which is derived from the value of ε_d by letting $\phi_4=\pi/2$.

$$\sin^2\phi_4 = \frac{\varepsilon_\parallel^3(\varepsilon_d - \varepsilon_\perp^*)}{(\varepsilon_\parallel - \varepsilon_\perp^*)\left[\varepsilon_d\varepsilon_\parallel^2 - \varepsilon_\perp^*(\varepsilon_\parallel - \varepsilon_d)^2\right]}. \tag{12}$$

When $1<\varepsilon_d\leq\chi$, the DSWs exist within a AED of $\phi_3<\phi\leq\phi_4$ while the DSWs exist within a AED of $\phi_3<\phi\leq\pi/2$ under $\chi<\varepsilon_d<-\varepsilon_\perp{}^*$.

3. Dyakonov surface waves at dielectric-elliptic type interface

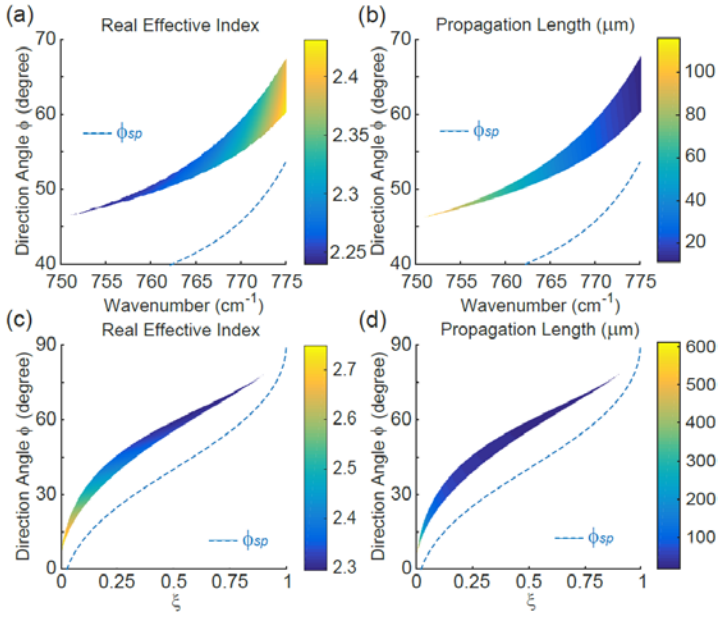

Figure 2. Dependencies of the real effective index and propagation length of the DSWs at the interface of dielectric-elliptic type on the wavenumber, the direction angle and the permittivity of isotropic dielectric material. The results of ϕ_{sp} are presented via dashed blue lines.

As presented in the previous section, the propagation of DSWs at the dielectric-elliptic interface could be theoretically described via Eqs.(1-10). In this section we present the results from

theoretical calculation. Firstly, the real effective index and propagation lengths of the DSWs as functions of the wavenumber, the direction angle of wave vector and the permittivity of isotropic dielectric material are studied and the results are shown in Fig. 2. According to the requirement of the existence of DSWs at the interface, *i.e.* $\varepsilon_{\parallel} > \varepsilon_d > \varepsilon_{\perp}$, the frequency span in Figs. 2(a-b) is chosen as 750 cm^{-1}<ω<775 cm^{-1} and the permittivity is set as $\varepsilon_d = (\varepsilon_{\perp}+\varepsilon_{\parallel})/2$. To study the influence of permittivity of isotropic dielectric on the propagation of DSWs, in Figs. 2(c-d) we define a quantity ξ with its value between 0 and 1. Therefore the permittivity ε_d can be expressed through $\varepsilon_d=\varepsilon_{\perp}+\xi(\varepsilon_{\parallel}-\varepsilon_{\perp})$. As quantity ξ spans from 0 to 1, the wavenumber is fixed at ω=770 cm^{-1}. For better presentation, we have also illustrated the results of ϕ_{sp}.

As shown in Fig. 2, the AED is quite narrow due to the tiny birefringence. The AED increases with the wavenumber within the whole wavelength span while increases first as the permittivity ε_d increases, achieving a maximum value and then decreases as the ε_d approaches to $\varepsilon_{\parallel}$. Meanwhile, both the lower and upper direction angle limits keep increasing as the wavenumber or quantity ξ increases. Furthermore, it can be also observed that the influence of permittivity ε_d on the direction angle is much stronger than the one of wavenumber. For instance, within the whole spectral range, the variation of upper limit ϕ_2 is nearly 20 degrees in Fig. 2(a) while almost 90 degrees in Fig. 2(c). It should be noted that, the AED is so narrow that it cannot be clearly observed for the wavenumber near ω=750 cm^{-1} or for the quantity near ξ=1. The detailed discussions concerning about the direction angle are presented in the next figure. As for the real effective index, it is quite small and stays nearly unchanged within the whole spectrum range, which means the DSWs are weakly confined at the interface. This weak confined property leads to an ultra-long propagation length, which can be over 600 μm when the permittivity ε_d approaches to $\varepsilon_{\perp}$. The propagation length decreases as the wavenumber or the quantity ξ increases, which can be attributed to either the higher loss of $\varepsilon_{\parallel}$ as wavenumber approaches to ω=775 cm^{-1} or the much higher loss of $\varepsilon_{\parallel}$ than $\varepsilon_{\perp}$ [not shown in Fig.1(b), but can be obtained straight-forward from Eq. (1)]. Meanwhile, it should be noted that, for the groups of parameters we choose, the curves of ϕ_{sp} (the blue dashed lines) stay outside the AED.

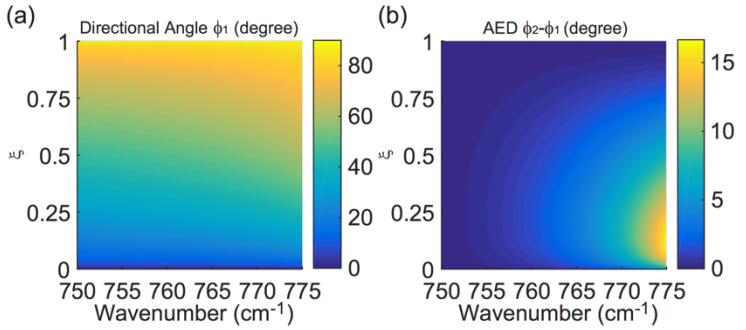

Figure 3. Dependencies of the lower direction angle limit ϕ_1 (a) and the AED ϕ_2-ϕ_1 (b) on quantity ξ and wavenumber.

To provide a deeper insight into the variation of AED of wave vector of DSWs, we respectively plot the direction angle limit ϕ_1 and the AED ϕ_1-ϕ_2 as functions of quantity ξ and wavenumber in Figs. 3(a) and 3(b). In Fig. 3(a) we observe that the influence of permittivity ε_d on lower direction angle limit ϕ_1 is much stronger than that of wavenumber, which could also be observed in Fig. 2. As the quantity increases from ξ=0 to ξ=1, the change of angle ϕ_1 is almost 90 degrees, in contrast to the change of angle ϕ_1 of only 14 degrees under various wavenumbers. The narrow AED of propagation of DSWs can be directly observed from Fig. 3(b), wherein the widest AED is slightly larger than 16°. The larger AED is achieved at larger wavenumber due to the larger birefringence in h-BN crystal [see Fig. 1(b)]. In addition, an optimized permittivity of

isotropic dielectric material exists for every wavenumber with the similar phenomenon has been observed in previous theoretical study [24]. Thus in experimental study of DSWs, the permittivity of the isotropic material should be carefully selected.

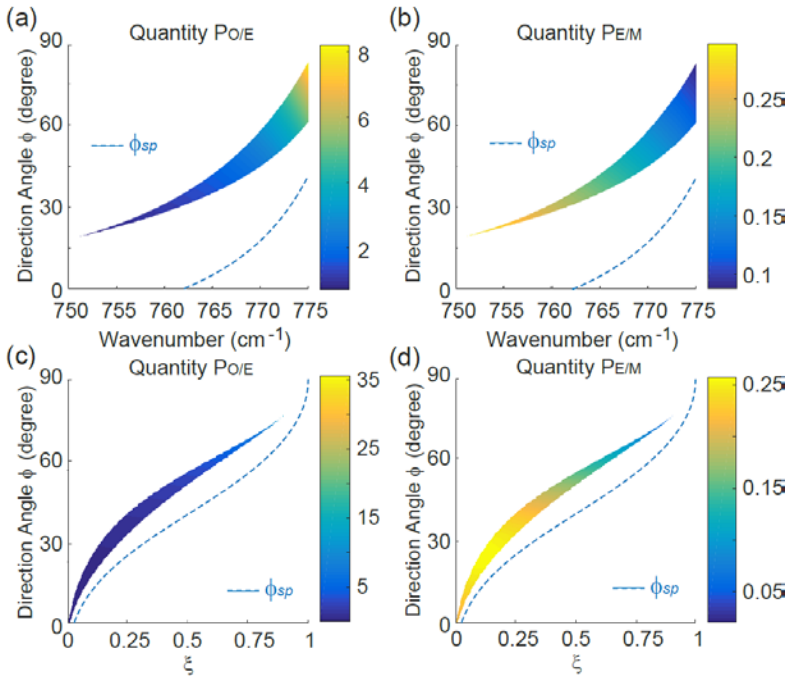

Figure 4. Dependencies of the quantities $P_{E/M}$ and $P_{O/E}$ on the wavenumber, the direction angle ϕ and the quantity ξ representing the permittivity of isotropic dielectric material. The results of ϕ_{sp} are presented via dashed blue lines.

It is well known that the DSWs are hybrid modes which combines four evanescent fields in isotropic dielectric and h-BN crystal [31]. To provide a better understanding on the modes hybridizing characteristic of DSWs, the two predefined quantities $P_{O/E}$ and $P_{E/M}$ as functions of the wavenumber, the direction angle ϕ and the quantity ξ are presented in Fig. 4. Again for the convenience of comparison, the curves corresponding to the direction angle ϕ_{sp} are presented. As for the presented theoretical results, it is easily found that the ordinary modes are dominant in h-BN crystal while the transverse-magnetic (TM) modes are dominant in the isotropic dielectric material. Furthermore, by comparing the influences of wavenumber and quantity ξ on $P_{O/E}$ and $P_{E/M}$, we note that the quantity ξ causes stronger influences than the wavenumber. As for the quantity $P_{O/E}$ itself, higher $P_{O/E}$ is obtained under larger direction angle ϕ, wavenumber or quantity ξ. The maximum $P_{O/E}$ over 35 is obtained as ξ and ϕ respectively approaches to ξ=1 and ϕ=90. For the other quantity, similar to the case of $P_{O/E}$, smaller $P_{E/M}$ is achieved under larger direction angle ϕ, wavenumber or quantity ξ with the minimum $P_{E/M}$ is below 0.03.

4. Dyakonov surface waves at dielectric-hyperbolic type interface

In the previous section, we have investigated the propagation of DSWs at dielectric-elliptic type interface. Although the DSWs exhibit a ultra-long propagation length, the AED is quite narrow (up to only 16°) due to the tiny birefringence within the elliptic region of h-BN. Therefore, it is essential to investigate the propagation of DSWs at dielectric-hyperbolic type interface since the hyperbolic dispersion enables a much larger birefringence and consequently a much wider AED of DSWs. Similar to Fig. 2 in previous section, we have presented in Fig. 5 the real effective index and propagation lengths of DSWs at the interface of dielectric-hyperbolic type as functions

of the wavenumber, the direction angle ϕ and the quantity ξ. In Figs. 5(a) and 5(b), the permittivity of isotropic dielectric material is chosen as $\varepsilon_d = \chi = -\varepsilon_{\parallel}\varepsilon_{\perp}^{*}/(\varepsilon_{\parallel}-\varepsilon_{\perp}^{*})$ and in this case the upper limit of direction angle is set as $\pi/2$ while the lower limit of directional angle is ϕ_3. Meanwhile the wavenumber in Figs. 5(c) and 5(d) is set as ω=1480 cm^{-1}. Note that in these two figures the definition of quantity ξ is different to that in the previous section. The quantities ξ is defined via the relationship $\varepsilon_d=1+\xi(-\varepsilon_{\perp}^{*}-1)$, which makes the ε_d varies from ε_d=1 to $\varepsilon_d=-\varepsilon_{\perp}^{*}$ as the quantity changes from ξ=0 to ξ=1. For a better presentation, the propagation length is presented in log scale.

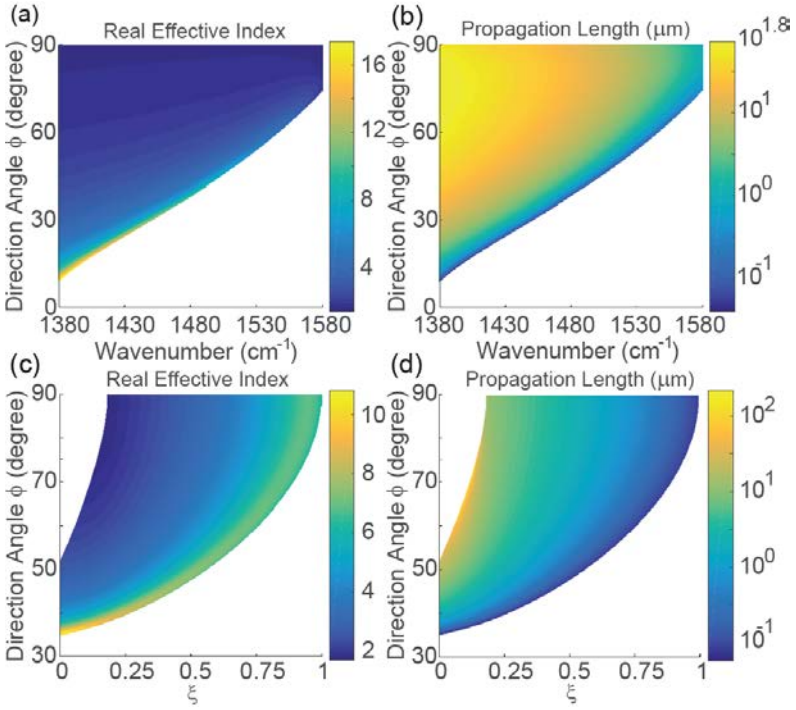

Figure 5. Dependencies of the real effective index and propagation length of the DSWs at the interface of dielectric-hyperbolic type on the wavenumber, the direction angle ϕ and the quantity ξ.

Compared with the case of dielectric-elliptic type of interface, the DSWs at the dielectric-hyperbolic type of interface exhibits a higher real effective index over 16 and a smaller propagation length over 150 μm. As shown in Fig. 5(a), the real effective index increases as wavenumber or direction angle decreases. Meanwhile, the AED decreases as the wavenumber increases, from nearly 80° at ω=1380 cm^{-1} to nearly 15° at ω=1580 cm^{-1}. In Fig. 5(b) the propagation length for arbitrary direction angle keeps decreasing with the increasing of wavenumber. In contrast, for every wavenumber, an optimized direction angle exists where the propagation length is maximum. In Figs. 5(c) and 5(d), two stages could be observed concerning the dependences of real effective index and propagation length on wavenumber. This can be attributed to the existence of permittivity χ during the variation of ε_d. For the permittivity located between the permittivities of ε_d=1 and $\varepsilon_d=\chi$, the AED is set as $\phi_3<\phi\leq\phi_4$ while for the one between the permittivities of $\varepsilon_d=\chi$ and $\varepsilon_d=-\varepsilon_{\perp}^{*}$, the AED turns into a different domain of $\phi_3<\phi<\pi/2$. Specifically, the real effective index increases and the propagation length decreases as the quantity ξ increases. On the other hand, the real effective index becomes higher at smaller direction angle with a shorter propagation length. Following a similar procedure as Fig. 3, we plot the lower limit of direction angle ϕ_1 and the AED ϕ_2-ϕ_1 as functions of wavenumber and the quantity ξ. The results are presented in Figs. 6(a) and 6(b), respectively.

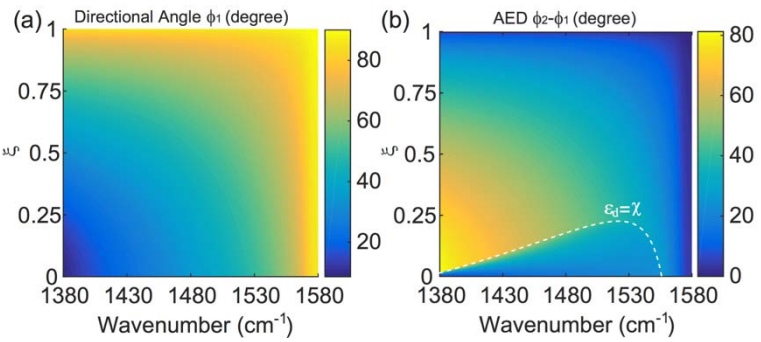

Figure 6. Dependencies of the lower direction angle limit ϕ_1 (a) and the AED ϕ_2-ϕ_1 (b) on quantity ξ and wavenumber.

In Fig. 6(a) the trends of curves corresponding to direction angle limit ϕ_1 are similar to those in the Fig. 3, namely the angle limit ϕ_1 increases with the wavenumber or the quantity ξ. Again in this case a variation range of 90 degrees can be achieved in the whole variation range of quantity or wavenumber. In Fig. 6(b) obvious discontinuity can be observed. This boundary corresponds to the position where the permittivity ε_d equals to the value of χ and the upper direction angle limit equals to $\pi/2$. To reveal this, the positions where $\varepsilon_d=\chi$ have been theoretically calculated and illustrated through white dashed line. As shown in the figure, the white dashed line is located exactly at the boundary of discontinuity. For the region surrounded by the dashed line of $\varepsilon_d=\chi$, the AED stays nearly unchanged. In contrast, for the region outside the discontinuity, the AED decreases as the wavenumber or quantity ξ increases. The largest AED over 80° is obtained near ω=1380 cm^{-1} and ξ=0. Thus in the experimental investigation, both smaller wavenumber and quantity are preferred and the region surrounded by discontinuity curve should be avoided. Next we focus on the multiple evanescent fields hybridizing of DSWs at dielectric-hyperbolic interface. The two quantities $P_{O/E}$ and $P_{E/M}$ are respectively presented in Figs. 7(a,c) and 7(b,d).

With respect to the $P_{O/E}$ under various wavenumbers, quantities ξ and direction angles ϕ, the influence of direction angle ϕ on $P_{O/E}$ is much strong than the other two factors. The variation of amplitude in $P_{O/E}$ can be more than two orders within the whole variation range of direction angle, in contrast to the only one order of amplitude variation within the full wavenumber span. Meanwhile, since most of the wave energy of extraordinary and ordinary modes is located in h-BN crystal, the effects of permittivity ε_d on the $P_{O/E}$ is much smaller than the two other factors, as shown in Fig. 7(c). As for the quantity $P_{E/M}$, there are always minimum $P_{E/M}$ existing in the whole span of wavenumber and quantity ξ. On the other hand, it can be observed that the whole region is divided by the curve of minimum $P_{E/M}$ into two different regions. For the region with smaller wavenumber, there is always a maximum $P_{E/M}$ existing within the whole span of direction angle. By contrast, for the region with smaller quantity ξ, the $P_{E/M}$ keeps decreasing as the direction angle decreases. On the other hand, for the regions with larger wavenumber or quantity ξ, the quantity $P_{E/M}$ increases as the direction angle decreases. By comparing Fig. 4 and Fig. 7, it is also found that the dielectric-hyperbolic type interface could cause a much obvious difference in the composition ratio between the two evanescent modes in either the h-BN crystal or the isotropic dielectric material.

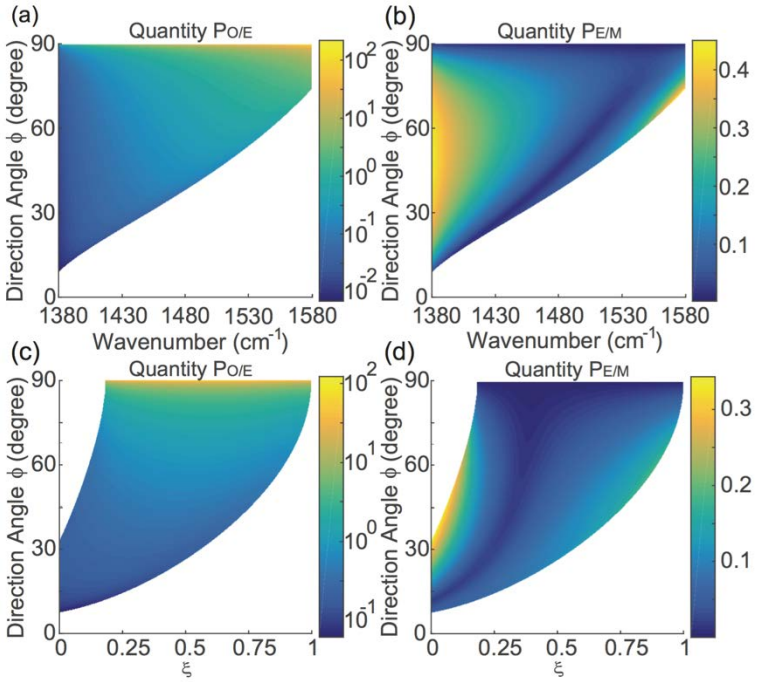

Figure 7. Dependencies of the quantities $P_{E/M}$ and $P_{O/E}$ of the DSWs in the isotropic dielectric material and the h-BN crystal on the wavenumber, the direction angle ϕ and the quantity ξ representing the permittivity of isotropic dielectric material.

The performances of DSWs at h-BN surface are also different to those in previous paper [24]. Firstly, the operation wavelength of DSWs at dielectric-elliptic or dielectric-hyperbolic type interface stays within the far-infrared wavelength region (12.9 μm<λ<13.3 μm) or mid-infrared wavelength region (6.3 μm<λ<7.2 μm). In contrast, the operation wavelength of DSWs was not specified in previous paper [24]. Secondly, the AED of DSWs at the surface of h-BN of elliptical dispersion (almost 16°) is narrower than that of Case 1 (almost 20°) in previous paper, wherein the metamaterial is assumed as the anisotropic substrate. However, the AED at the surface of h-BN with hyperbolic dispersion is much wider than that of Case 2 (less than 1°), wherein TiO_2 crystal is the anisotropic substrate [24]. Concerning the dielectric-hyperbolic type interface, the AED of DSWs at the surface of h-BN (up to 80°) is much larger than the counterpart (up to 45°) on hyperbolic uniaxial medium [24]. The superior property of AED on h-BN surface is attributed to its stronger isotropy or hyperbolicity at resonance frequencies.

5.Conclusions

In this paper, we investigate the propagation of DSWs at the interface between h-BN crystal and an isotropic dielectric material. The investigation is composed of two different types of interface, the dielectric-elliptic interface and the dielectric-hyperbolic interfaces. With respect to the modal performances, the DSWs at dielectric-elliptic interface exhibit a real effective index between two and three with a long propagation length up to 600 μm. Higher propagation length can be obtained at the smaller wavenumber, the quantity ξ or the direction angle. In contrast, the DSWs at the dielectric-hyperbolic interface present a dozens of real effective index while in cost of a shorter propagation length near 100 μm. The lower wavenumber or quantity ξ is still preferred for a larger propagation length while the direction angle should be selected close to the optimized value. Regarding the angular existence domain (AED), the DSWs at dielectric-elliptic interface propagate with a quite narrow AED up to 16°, much smaller than the AED of 80° for DSWs at the dielectric-hyperbolic interface. In the former case, to obtain wider AED, a larger wavenumber

is preferred with the quantity should be chosen close to the optimized value. In the latter case, smaller quantity or wavenumber should be chosen alternatively. However, the parameters should avoid being located inside the region surrounded by the curve of $\varepsilon_d=\chi$. For the DSWs at both interfaces, the ordinary waves are dominant in h-BN crystal while the TM waves are dominant in the isotropic dielectric material, although the difference between the two evanescent field components in h-BN or isotropic dielectric material for dielectric-elliptic case is much smaller than the dielectric-hyperbolic case. The study in this paper may provide a deeper insight into the propagation of DSWs at the interface between h-BN and isotropic dielectric material and may have potentials in diverse applications, such as the high sensitivity stress sensing and optical sensing of various types of analytes infiltrating one or both of the two dielectric materials.

Acknowledgements

This work is supported in part by the National Natural Science Foundation of China (NSFC) (Grant Nos. 61178008, 61275092).

References

[1]J. A. Polo, A. Lakhtakia 2011 *Laser & Photonics Reviews* **5** 234-46.
[2]W. L. Barnes, A. Dereux, T. W. Ebbesen 2003 *Nature* **424** 824-30.
[3]R. Li, B. Zheng, X. Lin, R. Hao, S. Lin, W. Yin, E. Li, H. Chen 2017 *IEEE Journal of Selected Topics in Quantum Electronics* **23** 1-8.
[4]X. Lin, Y. Shen, I. Kaminer, H. Chen, M. Soljačić 2016 *Physical Review A* **94**
[5]X. Lin, R. Li, F. Gao, E. Li, X. Zhang, B. Zhang, H. Chen 2016 *Optics letters* **41** 681-4.
[6]R. Li, X. Lin, S. Lin, X. Zhang, E. Li, H. Chen 2016 *Carbon* **98** 463-7.
[7]J. D. Caldwell, I. Vurgaftman, J. G. Tischler, O. J. Glembocki, J. C. Owrutsky, T. L. Reinecke 2016 *Nature nanotechnology* **11** 9-15.
[8]J. D. Caldwell, L. Lindsay, V. Giannini, I. Vurgaftman, T. L. Reinecke, S. A. Maier, O. J. Glembocki 2015 *Nanophotonics* **4**
[9]W. J. Tomlinson 1980 *Optics letters* **5** 323.
[10]M. D., N. R. G., F. V. K. 1984 *Physica Scripta* **29** 269-75.
[11]M. D., M. D., T. H. 1984 *Physica Scripta* **30** 335-40.
[12]G. I. Stegeman, C. T. Seaton, J. Chilwell, S. D. Smith 1984 *Applied Physics Letters* **44** 830.
[13]M. I. D'yakonov 1988 *Zh Eksp Teor Fiz* **94** 3.
[14]O. Takayama, L.-C. Crasovan, S. K. Johansen, D. Mihalache, D. Artigas, L. Torner 2008 *Electromagnetics* **28** 126-45.
[15]O. Takayama, D. Artigas, L. Torner 2014 *Nature nanotechnology* **9** 419-24.
[16]O. Takayama, L. Crasovan, D. Artigas, L. Torner 2009 *Phys Rev Lett* **102** 043903.
[17]D. B. Walker, E. N. Glytsis, T. K. Gaylord 1998 *Journal of the Optical Society of America A* **15** 248.
[18]J. Gao, A. Lakhtakia, M. Lei 2010 *Physical Review A* **81**
[19]C. J. Zapata-Rodriguez, J. J. Miret, S. Vukovic, M. R. Belic 2013 *Optics express* **21** 19113-27.
[20]D. P. Pulsifer, M. Faryad, A. Lakhtakia 2013 *Phys Rev Lett* **111** 243902.
[21]J. D. Caldwell, A. V. Kretinin, Y. Chen, V. Giannini, M. M. Fogler, Y. Francescato, C. T. Ellis, J. G. Tischler, C. R. Woods, A. J. Giles, M. Hong, K. Watanabe, T. Taniguchi, S. A. Maier, K. S. Novoselov 2014 *Nature communications* **5** 5221.
[22]L.-C. Crasovan, D. Artigas, D. Mihalache, L. Torner 2005 *Optics letters* **30** 3075.
[23]L. C. Crasovan, O. Takayama, D. Artigas, S. K. Johansen, D. Mihalache, L. Torner 2006 *Physical Review B* **74**
[24]E. Cojocaru 2014 *Journal of the Optical Society of America B* **31** 2558.
[25]J. B. Khurgin 2015 *Nature nanotechnology* **10** 2-6.
[26]S. Dai, Z. Fei, Q. Ma, A. S. Rodin, M. Wagner, A. S. McLeod, M. K. Liu, W. Gannett, W. Regan, K. Watanabe, T. Taniguchi, M. Thiemens, G. Dominguez, A. H. Castro Neto, A. Zettl, F. Keilmann, P. Jarillo-Herrero, M. M. Fogler, D. N. Basov 2014 *Science* **343** 1125-9.

[27]P. Li, M. Lewin, A. V. Kretinin, J. D. Caldwell, K. S. Novoselov, T. Taniguchi, K. Watanabe, F. Gaussmann, T. Taubner 2015 *Nature communications* **6** 7507.
[28]A. Kumar, T. Low, K. H. Fung, P. Avouris, N. X. Fang 2015 *Nano letters* **15** 3172-80.
[29]L. Song, L. Ci, H. Lu, P. B. Sorokin, C. Jin, J. Ni, A. G. Kvashnin, D. G. Kvashnin, J. Lou, B. I. Yakobson, P. M. Ajayan 2010 *Nano letters* **10** 3209-15.
[30]Y. Cai, L. Zhang, Q. Zeng, L. Cheng, Y. Xu 2007 *Solid State Communications* **141** 262-6.
[31]R. Li, C. Cheng, F.-F. Ren, J. Chen, Y.-X. Fan, J. Ding, H.-T. Wang 2008 *Applied Physics Letters* **92** 141115.